A novel in situ method for simultaneously and selectively measuring AsIII, SbIII, and SeIV in freshwater and soils

Fang, W., Yang, Y., Williams, P. N., Sun, H., Chen, H., Yang, D., Shi, X., Fu, R., & Luo, J. (2022). A novel in situ method for simultaneously and selectively measuring AsIII, SbIII, and SeIV in freshwater and soils. *Analytical Chemistry*, *94*(11), 4576-4583. https://doi.org/10.1021/acs.analchem.1c04243

Published in:
Analytical Chemistry

Document Version:
Peer reviewed version

A novel *in situ* method for simultaneously and selectively measuring As^{III}, Sb^{III}, and Se^{IV} in aquatic and terrestrial environment

Wen Fang[1], Yi Yang[1], Paul N. Williams[2], Haitao Sun[1], Haiyi Chen[1], Danxing Yang[1], Xinyao Shi[1], Rongbing Fu[3,4,5], Jun Luo[1]*

[1]State Key Laboratory of Pollution Control and Resource Reuse, School of the Environment, Nanjing University, Jiangsu 210023, China

[2]Institute for Global Food Security, School of Biological Sciences, Queen's University Belfast, Belfast BT9 7BL, United Kingdom

[3]State Key Laboratory of Pollution Control and Resources Reuse, College of Environmental Science and Engineering, Tongji University, Shanghai 200092, China

[4]Centre for Environmental Risk Management and Remediation of Soil and Groundwater, Tongji University, Shanghai 200092, PR China

[5]Shanghai Institute of Pollution Control and Ecological Security, Shanghai 200092, PR China

* Corresponding authors, 0086-25-89680623, esluojun@nju.edu.cn

■ ABSTRACT

Anthropogenic and climatic perturbations redistribute arsenic (As), antimony (Sb), and selenium (Se) within the environment. The speciation characteristics of these elements determine their behaviour and biogeochemical cycling, but these redox sensitive species are challenging to capture, with few methods able to harmonise measurements across the whole plant-soil-ecosystem continuum. In this study, we developed a novel DGT method based on aminopropyl and mercaptopropyl bi-functionalized mesoporous silica spheres (AMBS) to achieve *in-situ*, simultaneous, and selective quantification of As^{III}, Sb^{III}, and Se^{IV}, three typical/toxic, but difficult to measurement inorganic species. When used for environmental monitoring within a river catchment, AMBS-DGT exhibited stable/accurate predictions of these species despite varying water chemistries (ionic strength 0.01–200 mmol L^{-1} NO_3^-, pH 5–9 for As^{III} and Sb^{III}, and pH 5–7.5 for Se^{IV}). Further, river deployments also showed that time-averaged species concentrations by AMBS-DGT were reproducible compared with high-frequency sampling and measurement by HPLC-ICPMS. When AMBS-DGT was used for sub-mm scale chemical imaging of soil solute fluxes, the method resolved concomitant redox-constrained spatial patterns of As^{III}, Sb^{III}, and Se^{IV} associated with root O_2 penetration within anaerobic soil. Improved capabilities for measurement of compartment interfaces and microniche features are critical alongside the measurement of larger scale hydrological processes that dictate the fine-scale effects, with the AMBS-DGT achieving this for As^{III}, Sb^{III}, and Se^{IV}.

■ INTRODUCTION

Anthropogenic activities, such as mining and coal combustion, have caused severe arsenic (As), antimony (Sb), and selenium (Se) pollution in the environment.[1-3] For example there is widespread multi-metalloid damage in Hunan and Hubei provinces (South China) where there has been extensive Se-Sb ore extraction and processing.[4, 5] Additionally, coal combustion for power and heat generation have released large quantities of As, Sb, and Se to the atmosphere.[6] These transport processes are often difficult to be monitored and predicted, with the subsequent wet and dry deposition of the metalloids potentially enriching/polluting other environmental media, such as soils and sediments.[7]

To understand the biogeochemical cycling of As, Sb, and Se, their speciation distribution and transformation at different scales need to be studied.[8-10] Speciation measurements of As, Sb, and Se at the large-scale (metre to hectometre) are needed to quantify the pollution level and ecosystem toxicity.[11] However, underlying the ecosystem-scale response, the effect of biogeochemical processes at small-scale (nano- to micrometre) are always significant.[8, 12-14] Being susceptible to redox change, As, Sb, and Se speciation transformation are likely to occur at the anoxic-oxic interfaces as well as the hotspots where redox-active metastable phases are potentially involved.[15-17] For example, the radial oxygen loss (ROL) from rice roots leads to a steep change of redox condition in the rice-root interface, thereby posing significant impacts on speciation of As and the transfer of As between soils and plants.[15, 18]

Appropriate field techniques that are able to determine the spatial distribution of As, Sb, and Se speciation at both large-scale and small-scale, are required to understand their biogeochemical cycling.[19] Since the speciation of elements are greatly affected by media's properties (such as pH, redox condition, and availability of reactive adsorption surfaces), the sample collection and storage processes of traditional *ex-situ* measurement often introduce major uncertainties to the speciation determination.[20] Also, the subsequent speciation analysis after sampling is normally conducted using high performance liquid chromatography (HPLC) coupled with inductive coupled plasma mass spectroscopy (ICP-MS). However, the different column and mobile phase requirements of HPLC separation make the simultaneously detection of multi-species/elements mixtures in a single analysis difficult. Recently, the passive sampling technique of diffusive gradients in thin-films technique (DGT) has emerged as an effective/suitable tool for low-disturbance and *in situ* speciation measurement in a range of different environment media.[17, 21, 22] Moreover, if the material in the binding gel of the DGT device is very fine textured and homogeneously distributed, it can be used to measure pollutant bioavailability and speciation at critical environmental interfaces with resolutions of μm–mm.[17, 23]

The majority of DGT configurations are for total element capture, but there are some devices that have been developed for *in situ* selective measurement of some As, Sb, and Se species,[17, 21, 24, 25] respectively, and the detection limits of these DGT devices are comparable to, sometimes even more sensitive than HPLC-ICPMS. In this study,

for the first time, multi-species all-in-one DGT devices assembled with the binding gel made from aminopropyl and mercatopropyl bi-functionalized mesoporous silica sphere (AMBS) were developed for simultaneous measurement of three priority species: As^{III}, Sb^{III}, and Se^{IV}. These three typical inorganic species of As, Sb, and Se are of great concern due to their higher toxicity compared with their other forms.[3, 18, 26, 27] The simultaneous multi-elemental speciation measurement enabled by AMBS-DGT was analytically superior whilst conferring improvements in time/labor efficiency. Moreover, this homogeneous AMBS binding gel can achieve two dimensional visualization of As^{III} fluxes at the μ-scale, which can overcome the limitation of existing 3-Mercaptopropyl-functionalized silica (MFS) binding gel in the high-resolution mapping of As^{III} solute behaviors.[21]

Overall, performances of AMBS-DGT were evaluated for measuring As^{III}, Sb^{III}, and Se^{IV} under different conditions (i.e. pH, ionic strength, deployment time, elemental interference, and aging effect), and then the AMBS-DGT was compared with conventional water/grab sampling to validate its application in freshwater at the hectometer scale. Then, the AMBS binding gel was applied at the rice root-soil interface, a typical micro-scale scenario, to visualize the spatial patterns of As^{III}, Sb^{III}, and Se^{IV} lability around rice roots, which can be used to parametrize risk assessment and geochemical modelling of As, Sb, and Se biogeochemical behaviors at critical interface zones.

■ EXPERIMENTAL SECTION

Preparation and characterization of aminopropyl and mercatopropyl bi-functionalized mesoporous silica sphere (AMBS). AMBS, with the particle size of ~3.4 μm, was synthesized following some modification of the methods reported by Shi et al. (2018)[24], Aguado et al. (2008)[28], and Burke et al. (2009)[29]. These changes to the binder chemistries enabled the simultaneous and selective measurement of As^{III}, Sb^{III}, and Se^{IV}. The key production step modification was related to the specific molar ratio of mercaptopropyl to aminopropyl groups on the mesoporous silica surfaces, which controls the performance of AMBS-DGT in selective measurement of As^{III}, Sb^{III}, and Se^{IV}.

First, the mercaptopropyl functionalized mesoporous silica particle was obtained by co-condensation reactions using P123 ($EO_{20}PO_{70}EO_{20}$), 3-mercaptopropyl-trimethoxysilane (MPTMS, $C_6H_{16}O_3SSi$), and tetraethyl orthosilicate (TEOS). The molar ratio of MPTMS/(MPTMS + TEOS) was set at 0.3. Then, mercaptopropyl functionalized mesoporous silica solid was furtherly modified with 3-aminopropyl-trimethoxysilane (APTMS, $C_6H_{17}O_3NSi$) through post-synthesis reflux procedures to prepare aminopropyl and mercatopropyl bi-functionalized mesoporous silica particles. The supramolecular templates were removed using 95% ethanol extraction and the AMBS product was obtained after water wash, filtered, and vacuum dried at 45 °C for 24h. During AMBS preparation, the molar ratio of MPTMS to APTMS was controlled at 6-7 to ensure the molar ratio of mercaptopropyl to aminopropyl groups on the

mesoporous silica surfaces at 5:1.

Apart from AMBS, we also synthesized another two types of mesoporous silica sphere (SBA-I and SBA-II) based on the approach reported by Fang et al. (2020)[17] and Shi et al. (2018)[24] to compare their ability in simultaneously and selectively measuring As^{III}, Sb^{III}, and Se^{IV}. SBA-I, just containing thiol groups and not amino groups, was validated to be feasible in selectively measuring Sb^{III} and prepared according to Fang et al. (2020)[17]. SBA-II, similar to AMBS, with both thiol and amino groups, has been reported to possess the ability to selectively measuring Se^{IV}[24]. However, the molar ratio of thiol groups to amino groups was lower for SBA-II (1.4:1) compared with AMBS (5:1). The AMBS, SBA-I, and SBA-II were characterized using X-ray photoelectron spectra (XPS, PHI5000, Japan) to analyze the chemical states of surface elements and confirm thiol and amino group functionalization (Figure 1).

DGT preparation. Standard piston DGT devices (exposure window area of 3.12 cm^2, DGT Research Ltd., UK), consisting of a binding gel layer, a diffusive gel layer, and a 0.45 μm pore size polyether sulfone (PES) filter membrane (Pall, USA), were used in this study. First, acrylamide based gel solution containing 37.5% acrylamide (Electron, BDH) (w/v), 47.5% Milli-Q water (18.2 MΩ·cm, Millipore, USA) (w/v), and 15% agarose-derived cross-linker (DGT Research Ltd., UK) (w/v) was prepared for making the diffusive and binding gels. Then, polyacrylamide diffusive gels (0.8 cm thickness) were cast according to Zhang and Davison.[30, 31] The binding gel was made from solid resin particles (including AMBS, SBA-I, and SBA-II) and gel solution. 0.2

147 g (dry weight) of the solid resin particles were added to 3 mL of the gel solution. After
148 the mixture was stirred well, 24 μL of 10% ammonium persulphate solution (AnalaR,
149 BDH) and 8 μL of *N,N,N'N'*-tetramethyl ethylenediamine (TEMED, 99%, Merck,
150 Germany) were added and mixed well. Finally, the gel solution mixture was cast
151 between two acid-cleaned glass plates, separated by a 0.25 mm thick spacer, and then
152 incubated in an oven at 45 °C for 45 min. To prepare the ultrathin binding gel, the same
153 procedure was employed, however a 50 μm-thick spacer was used. The solidified gel
154 was fully hydrated with Milli-Q water and washed using Milli-Q water for 2-3 times in
155 24 h, resulting in a hydrated binding gel of 0.4 mm thickness.

156 **Uptake Kinetics of As^{III}, Sb^{III}, and Se^{IV}.** Uptake kinetics of As^{III}, Sb^{III}, and Se^{IV}
157 by binding gels made from AMBS, SBA-I, and SBA-II were investigated by exposing
158 gel discs (2.5 cm diameter) to 10 mL of 10 mM $NaNO_3$ solution (pH ~5.70) containing
159 ~50 μg L^{-1} As^{III}, Sb^{III}, and Se^{IV} or As^{V}, Sb^{V}, and Se^{VI}. Triplicate binding gel discs were
160 immersed in the mixed solution and shaken for various time from 10 min to 24 h. The
161 adsorption efficiencies of As, Sb and Se species by AMBS, SBA-I, and SBA-II binding
162 gel discs were calculated by the difference between their initial concentrations and final
163 concentrations in the immersion solution.

164 **Effects of ionic strength and pH.** Due to the variability of ionic strength and pH
165 in the environment, AMBS-DGT performance must be evaluated across a wide range
166 of ionic strength and pH. Generally, triplicate AMBS-DGTs were deployed for about 4
167 h at ~25 ºC in various well stirred solutions: (a) 2 L of mixed solutions containing 50

168 μg L^{-1} As^{III}, Sb^{III}, and Se^{IV} with $NaNO_3$ concentration ranging from 0–200 mM with
169 pH ~5.60 and (b) 2 L of 10 mM $NaNO_3$ solutions containing 50 μg L^{-1} As^{III}, Sb^{III}, and
170 Se^{IV} with pH 3–10. Concentrations of target elements measured using DGT based on
171 Eq. S4, C_{DGT}, were compared with the solution concentrations directly determined by
172 ICP-MS, C_{soln}, to calculate the ratio of C_{DGT}/C_{soln}, evaluating the accuracy of AMBS-
173 DGT to measure As^{III}, Sb^{III}, and Se^{IV}.

174 Considering that positively charged amino functionalized groups on AMBS have
175 the potential to bind negatively charged As^{V}, Sb^{V}, and Se^{VI} especially under acidic pH,
176 the influence of pH on the accumulation of As^{V}, Sb^{V}, and Se^{VI} in AMBS-DGT was
177 evaluated to ensure whether these DGT devices can remain selective for As^{III}, Sb^{III}, and
178 Se^{IV} over a range of environmentally relevant pH. Generally, triplicate AMBS-DGTs
179 were deployed for ~4 h in 2 L of well-stirred solutions containing 50 μg L^{-1} of As^{V}, Sb^{V},
180 and Se^{VI} with a matrix of 10 mM $NaNO_3$ and pH 3–7.5 at ~25 °C. The ratio of C_{DGT}/C_{soln}
181 of As^{V}, Sb^{V}, and Se^{VI} was obtained to evaluate their adsorption by AMBS-DGT.

182 **Long time deployment.** The performance of selective measurement of As^{III}, Sb^{III},
183 and Se^{IV} by AMBS-DGT devices were further evaluated over a deployment time of 72
184 h. The AMBS-DGT devices (n=21) were immersed in 6 L of 10 mM $NaNO_3$ solution
185 (pH: ~5.50–5.60) containing ~50 μg L^{-1} of As^{III}, Sb^{III}, and Se^{IV} or As^{V}, Sb^{V}, and Se^{VI}
186 and then retrieved in triplicate at deployment times of 4, 6, 8, 12, 24, 48, and 72 h. 1%
187 NaN_3 was added to the solution to avoid possible microbe-catalyzed speciation change.
188 The accumulation of As, Sb, and Se by AMBS-DGT as a function of time were plotted.

Capacity and Aging Effect. To determine the capacity of AMBS binding gels to linearly and quantitatively accumulate As^{III}, Sb^{III}, and Se^{IV} according DGT theory (see the part of Principle of DGT in the supporting information), AMBS-DGT devices were deployed in 2 L of well-stirred 0.01 mol L^{-1} $NaNO_3$ solutions containing As^{III}, Sb^{III}, and Se^{IV} ranging from 0.1 to 20 mg L^{-1} with pH being adjusted to ~6.0. Notably, the adsorption capacity of AMBS-DGT were conducted separately for As^{III}, Sb^{III}, and Se^{IV}. Here, the capacity referred to the highest DGT-accumulated mass agreeing with the predicted mass based on Eq. S4. To investigate the effect of aging of the AMBS binding gels on the performance, the AMBS binding gels were stored at 4°C in 0.01 mol L^{-1} $NaNO_3$ for up to 140 d after production. DGT devices containing these AMBS binding gels with different aging time were deployed in 2 L of well-stirred 0.01 mol L^{-1} $NaNO_3$ solutions containing 50 μg L^{-1} As^{III}, Sb^{III}, and Se^{IV} for 4 h. Then, C_{DGT}/C_{soln} was calculated to evaluate the performance of AMBS-DGT with different aging time.

Interference of As^{V}, Sb^{V}, and Se^{VI} on AMBS-DGT performances. Considering that As^{III}/As^{V}, Sb^{III}/Sb^{V}, and Se^{IV}/Se^{VI} are common species of As, Sb, and Se in the real environmental scenarios, possible interference of As^{V}, Sb^{V}, and Se^{VI} on AMBS-DGT performance of measuring As^{III}, Sb^{III}, and Se^{IV} was evaluated by deploying AMBS-DGT in the 0.01M $NaNO_3$ solution (pH: ~5.50) containing both As^{V} and As^{III} (or Sb^{V} and Sb^{III}, or Se^{VI} and Se^{IV}). Concentration ratios of As^{V}/As^{III} (or Sb^{V}/Sb^{III}, or Se^{VI}/Se^{IV}) was set from 1 to 10, representing the common range of As^{V} and As^{III} (or Sb^{V} and Sb^{III}, or Se^{VI} and Se^{IV}) fractionations in real environments. The concentrations of As^{III}, Sb^{III},

and Se^{IV} kept stable at ~50 μg L^{-1}. Triplicate AMBS-DGTs were deployed in the mixed solutions for 4 h and the AMBS binding gels in the retrieved DGTs were eluted in 3 mL of 1 M HNO_3 + 1% KIO_3 (m/v) for ~24 h prior to ICP-MS analysis. Subsamples of the mixed deployment solutions were collected and stored at -20 ºC before speciation analysis of As, Sb, and Se using HPLC (Flexar, PerkinElmer, US) coupled with ICP-MS, as described in the Supporting Information.

***In situ* deployment of AMBS-DGT in freshwater.** AMBS-DGT devices were deployed at a sampling site (32°2'46" N, 118°48'37" E) from Jul. 4, 2019 to Jul. 16, 2019 in the Qinhuai River, a main river in Nanjing city, Jiangsu, China to test the applicability and the robustness of AMBS-DGT for measuring As^{III}, Sb^{III}, and Se^{IV} in a real aquatic system. The Qinhuai River is a tributary to the Yangtze River flowing through an urban area with a population of 8 million.[32] AMBS-DGTs in triplicate, together with a temperature data logger (iButton DS1921G, Maxim, USA) set to record water temperature at intervals of 2 h, were placed about 50-100 cm below the water surface on July 4th, July 7th, July 10th, and July 13th, and then collected after a deployment time of 72 h. Water samples were collected every 3 days during the experiment and stored at -20 ºC prior to As, Sb, and Se speciation analysis using HPLC-ICP-MS.

Chemical mapping of As^{III}, Sb^{III}, Se^{IV} in the rhizosphere. In this study, ultrathin/HR AMBS binding gels were exposed to preflooded and conditioned rice rhizotrons, achieving the 2D spatial visualization of labile fluxes of As^{III}, Sb^{III}, and Se^{IV}.

Labile fluxes (pg cm^{-2} s^{-1}) were mainly determined by the labile concentration adjacent to the gel surface and calculated based on the accumulation mass of metals in the gel and the deployment time. Details on the preparation of soils and rhizotrons are described in the Supporting Information. Briefly, after 3 weeks of rice cultivation in the rhizotrons, the AMBS binding gel was deployed to the soil for 24 h. The accumulation of target elements in the gels will be expressed as labile fluxes (Figure S1) measured using LA (Laser Ablation)-ICP-MS (New Wave UP-213(Nd-YAG)) (the Supporting Information).

■ RESULTS AND DISCUSSION

Uptake kinetics. Adsorption between thiol groups and As^{III}, Sb^{III}, and Se^{IV} is the basis for the selective measurement of these species.[21, 24, 25] AMBS binding gels rapidly adsorb As^{III}, Sb^{III}, and Se^{IV} (Figure 2), with uptake ratios of 74.4%, 95.3%, and 89.9%, respectively, within 60 min. The binding rate over the first 30 min was about 1.35 ng min^{-1} cm^{-2} for As^{III}, 2.30 ng min^{-1} cm^{-2} for Sb^{III}, and 1.87 ng min^{-1} cm^{-2} for Se^{IV}. The binding rate was much higher than the diffusion flux (0.56 ng min^{-1} cm^{-2} for As^{III}, 0.61 ng min^{-1} cm^{-2} for Sb^{III}, and 0.52 ng min^{-1} cm^{-2} for Se^{IV}) calculated from AMBS–DGT devices (domain diffusion thickness: 0.89 mm) which were assumed to be deployed in 100 μg L^{-1} As^{III}, Sb^{III}, and Se^{IV} solutions at 25 °C. It suggests that AMBS gels can uptake As^{III}, Sb^{III}, and Se^{IV} rapidly to ensure its concentration at the interface between the binding gel and the diffusive gel being effective zero, meeting the basic requirement for the method development of DGT. In contrast, less than 5% of As^{V}, Sb^{V}, and Se^{VI}

252 were retained in the AMBS binding gels after 24-h adsorption. Selectivity for As^{III}, Sb^{III},
253 and Se^{IV} was due to the specific adsorption by thiol groups as well as the stronger
254 electrostatic adsorption between positively charged amino groups and negatively
255 charged reduced species.

256 Comparison of the AMBS, SBA-I, and SBA-II binding gels showed that the uptake
257 kinetic of SBA-II binding gel was similar to that of AMBS, but the adsorption ratio of
258 SBA-I binding gel for As^{III} and Se^{IV} were obviously lower (Figures 2 and S2). The
259 adsorption efficiency of SBA-I binding gels for As^{III} and Se^{IV} reached only 20–30% in
260 24 h. Different from AMBS and SBA-II which host thiol and amino groups, SBA-I is
261 only thiol functionalized. Figures 2 and S2 indicate that the existence of amino groups
262 in the absorbents greatly influence the adsorption rate of As^{III} and Se^{IV} by the binding
263 gels. When materials of 0.05 g AMBS and SBA-II were mixed with the As^{III} and Se^{IV}
264 solution with concentration of ~1000 μg L^{-1} for 30 min, the adsorption ratios of As^{III}
265 and Se^{IV} were 99.3±0.2% and 99.7±0.1%, while the corresponding values for SBA-I
266 were only 20.1±5.5% and 2.2±1.6%. First, AMBS and SBA-II functionalized with
267 amino groups had higher zeta-potential values (AMBS: -11.4 mV and SBA-II: -7.61
268 mV) than SBA-I (-23.6 mV), thereby posing higher adsorption for negatively charged
269 Se^{IV}.[33, 34] Second, introducing aminopropyl groups into mercaptopropyl-
270 functionalized hexagonal mesoporous silica can result in significant increase in the
271 hydrophilic character of the adsorbent[35], thereby increasing the adsorption rate and
272 capacities.

pH influence on AMBS-DGT performance. *Selectivity.* pH is a dominant factor influencing the selectivity of AMBS-DGT since positively charged amino groups in AMBS binding gels may adsorb negatively charged oxyanions As^{V}, Sb^{V}, and Se^{VI} through electrostatic bonding, especially in acidic conditions. Figure S3 shows the accumulation of As^{V}, Sb^{V}, and Se^{VI} in AMBS-DGT strongly depends on the solution pH. For AMBS-DGT when pH was >5.2, the C_{DGT}/C_{soln} ratios for As^{V}, Sb^{V}, and Se^{VI} were lower than 0.08. However, at pH 3, the C_{DGT}/C_{soln} for Sb^{V} and Se^{VI} increased to 0.46 and 0.28, respectively. Such phenomenon was also reported by Bennett et al. (2016)[25], using a DGT made by mercapto-silica (200–400 mesh, Sigma-Aldrich) (MFS-DGT) for selective measurement of Sb^{III}, but the adsorption for Sb^{V} with its C_{DGT}/C_{soln} increased from 0.16 to 0.82 when pH decreasing from 6.18 to 4.06. According to the requirement of C_{DGT}/C_{soln} <0.1, the pH range for negligible adsorption of As^{V}, Sb^{V}, and Se^{VI} were at pH>3.0, >4.1 and >5.2, respectively, for AMBS-DGT.

Compared with the DGT assembled with SBA-II binding gel which also measures As^{III}, Sb^{III}, and Se^{IV}, AMBS-DGT showed better selectivity. At pH 5.2, C_{DGT}/C_{soln} for As^{V} measured by SBA-II-DGT was 0.28, much higher than AMBS-DGT at 0.06, and the difference was even more significant as pH decreased (Figure S3). This was mainly attributed to the higher density of amino groups on SBA-II, providing greater adsorption of As^{V}, Sb^{V}, and Se^{VI}. The XPS core-level spectra of N1s for AMBS and SBA-II showed that $–NH_2^+–$/$–NH_3^+$ functionalization in SBA-II was much higher than AMBS although they had similar contents of –NH–/$–NH_2$ (Figure 1 and Table S1). The

higher density of positively charged $–NH_2^+–/–NH_3^+$ enhances the ability of SBA-II to adsorb negatively charged As^V, Sb^V, and Se^{VI} (such as $H_2AsO_4^-$, $Sb(OH)_6^-$, $HSeO_4^-$, and SeO_4^{2-}) via electrostatic bonding. Therefore, only at pH>6.0 can SBA-II-DGT keep its selectivity for As^{III} and Se^{IV}, this limited pH range makes it unsuitable for many environmental deployments. The better selectivity of AMBS-DGT than SBA-II-DGT furtherly emphases the necessity of lowering/optimizing the amino group density to ensure As^{III}, Sb^{III}, and Se^{IV} selectivity is maintained across a wide a pH as possible.

Accuracy. Good responses of AMBS-DGT to the deployment solution were found for As^{III} and Sb^{III} with C_{DGT}/C_{soln} of 1.0 ± 0.1 when solution pH was in the range of 3.9–9.1 (Figure 3). Even at lower (2.9) and higher pH (10.2), C_{DGT}/C_{soln} of Sb^{III} still kept in the acceptable limits of 1.0 ± 0.1. This working pH range was similar and sometimes wider when compared with that of DGT assemblies with MFS (5.0–8.2 for As^{III} and 7.00–8.05 for Sb^{III}).[21, 36]

For selective measurement of Se^{IV}, AMBS-DGT showed good responses to the solution concentration when pH was in the range 2.9–7.5 while it would underestimate the actual concentration of Se^{IV} at pH>7.5 since thiol-selenite reaction rates decrease rapidly once the pH exceeds 4.5.[37] The decreasing accumulation of Se at alkaline pH was also reported for SBA-II-DGT at pH>8.5 and Metsorb-DGT at pH>7. Shi et al. (2018)[24] illustrated that the amino functionalized groups on the surface of mesoporous silica can improve the adsorption ability for Se^{IV} at alkaline pH. To achieve accurate and selective measurement of Se^{IV}, SBA-II-DGT or AMBS-DGT can be chosen based

315 on the pH of real application scenarios. Overall, the novel AMBS–DGT device is
316 applicable for *in situ* As^{III} and Sb^{III} measurement in the environment with pH 4–9 and
317 Se^{IV} measurement with pH of 5–7.5 considering jointly selectivity and accuracy.

318 **Effects of ionic strength.** Effects of ionic strength on the DGT performance was
319 examined to ensure the application of AMBS-DGT in environmental relevant scenarios.
320 C_{DGT}/C_{soln} of As^{III}, Sb^{III}, and Se^{IV} were reproducible within acceptable limits of 1.0 ±
321 0.1 when the concentration of NO_3^- was in the range of 0.01–200 mM except Se^{IV} at
322 0.01 and 200 mM (Figure 3). This indicated that the AMBS-DGT can accurately
323 measure the concentrations of As^{III}, Sb^{III}, and Se^{IV} in most of natural waters with ionic
324 strength lower than 200 mM, such as fresh water and wastewater. Higher values (>1.1)
325 of C_{DGT}/C_{soln} for Se^{IV} was found at quite low NO_3^- concentration of 0.01 mM. Similar
326 irreproducibility has been observed for other elements at such low ionic strength[38, 39],
327 where the negligible screening accentuates effects associated with charges within the
328 acrylamide gel, such as Donnan partitioning.[38, 40]

329 **Accumulation over time and Capacities**. Selective measurement of As^{III}, Sb^{III},
330 and Se^{IV} by AMBS-DGT was further evaluated through deploying AMBS-DGT devices
331 in solutions containing either As^{III}, Sb^{III}, and Se^{IV} or As^{V}, Sb^{V}, and Se^{VI} for 72 h. The
332 accumulation of As^{III}, Sb^{III}, and Se^{IV} in AMBS-DGT increased linearly with the
333 increasing deployment time during 72 h and fitted well with the theoretical line
334 predicted from the know solution concentration using Eq. S4 (Figure S4). Nevertheless,
335 the accumulation of As^{V}, Sb^{V}, and Se^{VI} during a 72 h deployment was negligible,

336 furtherly validating the selectivity of AMBS-DGTs for As^{III}, Sb^{III}, and Se^{IV}.

337 Higher capacity can support the application of AMBS-DGT in scenarios with
338 higher concentrations of As^{III}, Sb^{III}, and Se^{IV} and longer deployment time. Here, the
339 capacity referred to the highest mass accumulated by DGT that agreed with the
340 predicted linear uptake based on Eq. S4. This capacity is not same as the maximum
341 mass from the perspective of gel adsorption since the accumulation of target elements
342 in the binding gel can still be higher, but are not relevant to the theoretical accumulation
343 mass. As shown in Figure S5, the accumulation masses of As^{III}, Sb^{III}, and Se^{IV} in
344 AMBS-DGT initially increased linearly with their solution concentrations and fitted
345 well with the theoretical line predicted by Eq. S4 based on the solution concentrations.
346 However, when the solution concentrations continued to increase, the accumulated
347 masses in DGT gradually deviated from the theoretical line due to the limited capacity.
348 As implied from Figure S5, the capacities of AMBS-DGT for As^{III}, Sb^{III}, and Se^{IV} are
349 ~21 μg, 34 μg, and 7.6 μg per gel disc (2.5 cm in diameter), respectively (Table S2). It
350 is true that the capacities were comparable to those reported for As^{III} (77.5 μg)[27] and
351 Sb^{III} (100 μg)[31] of MFS-DGT and Se^{IV} (25 μg) of SBA-DGT, but according to these
352 capacities, AMBS-DGT was feasible to be applied in most of natural environments with
353 As^{III}, Sb^{III}, and Se^{IV} concentrations lower than ~900 μg L^{-1}, ~1300 μg L^{-1}, and ~400 μg
354 L^{-1} based on the deployment time of 24 h. We can lower the deployment time or increase
355 the diffusive gel thickness when AMBS-DGT was applied in scenarios with quite high
356 concentrations of these species.

Interference of As^{V}, Sb^{V}, and Se^{VI} on AMBS-DGT performance. As shown in Table S3, when the concentration ratios of As^{V} to As^{III} (Sb^{V} to Sb^{III}, or Se^{VI} to Se^{IV}) increased from 1 to 10, C_{DGT}/C_{soln} of As^{III} and Sb^{III} kept within the range of 0.9–1.1. C_{DGT}/C_{soln} of Se^{IV} increased slightly to 1.2, but it is still acceptable for application in fields. These data indicate that the selectivity of AMBS-DGT for As^{III}, Sb^{III}, and Se^{IV} are almost free from the interference of As^{V}, Sb^{V}, and Se^{VI}.

Field trial of AMBS-DGT in freshwaters. AMBS-DGT was deployed in an inland river catchment to validate in situ measurements of As^{III}, Sb^{III}, and Se^{IV}. Concentrations of As^{III}, Sb^{III}, and Se^{IV} determined by AMBS-DGT deployed in the Qinhuai river were compared with companion grab sample measurements. AMBS C_{DGT} for Se^{IV} and Sb^{III} were lower than their respective detection limits (0.12 μg L^{-1} for Se^{IV} and 0.02 μg L^{-1} for Sb^{III}), which is consistent with the C_{soln} of Se^{IV} and Sb^{III} in grab samples which were collected at the same time and measured by HPLC-ICPMS (Table S4). Regarding As^{III}, C_{DGT}/C_{soln} was almost reproducible within the range of 1.0 ± 0.2 except for the AMBS-DGT devices collected in July 10, 2019 (Figure 4). The relatively low C_{DGT}/C_{soln} of 0.71 for the DGT devices deployed from July 7 to July 10 might be due to overestimation of C_{soln} induced by the steep change of As^{III} concentration during this period. As shown in Table S4, C_{soln} of As^{III} decreased from 1.35 μg L^{-1} collected on July 7 to 0.38 μg L^{-1} on July 10. Calculating C_{soln} based on the average concentration of these two samples cannot represent well the actual As^{III} concentration in waters during this deployment period, thereby causing deviation of C_{DGT}/C_{soln}.

Chemical mapping of As^{III}, Sb^{III}, and Se^{IV} in the rhizosphere. The spatial patterns of As^{III}, Sb^{III}, and Se^{IV} near rice roots were shown in Figure 5. The fine sizes (~3.4 μm) of AMBS made the binding gel to be homogenously distributed with the absorbents, thereby supporting the visualization of the change of As^{III}, Sb^{III}, and Se^{IV} labile flux within the microscale. 2D mapping of As^{III}, Sb^{III}, and Se^{IV} (Figure 5) shows depletion of As^{III} and Sb^{III} labile fluxes but the significant mobilization of Se^{IV} within rice rhizosphere. When we focused on the profile plots (Figure S8), it is obvious that in the zone of 2.5 mm away from the root surface, As^{III} labile flux gradually decreased from 0.18 pg cm^{-2} s^{-1} to 0.02 pg cm^{-2} s^{-1} approaching the root surface, but the Sb^{III} labile flux kept minima (~0.38 pg cm^{-2} s^{-1}) in the zone of 0-1.5 mm from the root surface. Compared with As^{III}, Sb^{III} is more sensitive to redox change and thereby could be oxidized by radial oxygen loss in the zone farer from the root surface. The maxima of Se^{IV} labile flux (~0.61 pg cm^{-2} s^{-1}) occurred in the zone ~0.5–1.5 mm from the root surface, but in the zone of 0.5 mm from the root surface, there was a decline of Se^{IV} labile flux, which might be attributed to the root uptake. The spatial distributions of Sb^{III} and Se^{IV} were similar to the profiles revealed by Fang et al. (2020)[17] and Shi et al. (2018)[24]. Furthermore, this is the first observation of the As^{III} flux distributions using HR DGT in the rice rhizosphere, with the decreasing labile flux of As^{III} in the zone of 0–2 mm from the root centre, overlapping with the aerobic rooting zone. As reported by previous studies, oxygenation is sustained most effectively around lateral root apices and young root tips, resulting in the formation of oxidized condition in these zones.[15,

[41] The oxidation of As^{III} and Sb^{III} as well as adsorption by Fe plaque will greatly lower their lability. However, the enhanced Se^{IV} labile flux might be related to phosphorus depletion in rhizosphere since it has been reported that Se^{IV} uptake by plant can be improved by phosphorus deficiency.[42] To reveal the underlying mechanisms controlling changes of species and lability of As, Sb, and Se in the rice rhizosphere, more investigations combining HR-DGT with other techniques, such as O_2 planar optode, are recommended.

■ CONCLUSIONS

The biogeochemical perspective, which is the detection and quantitative assessment of As, Sb, and Se speciation under *in situ* conditions at different spatial resolution, remains a challenge. The AMBS-DGT device developed in this study provides a uniform approach to measure the As^{III}, Sb^{III}, and Se^{IV}, three typical inorganic species of As, Sb, and Se, at both the small-scale (nano- to micrometre) and large-scale (metre to hectometre). AMBS-DGT exhibited stable and accurate measurement of As^{III}, Sb^{III}, and Se^{IV} throughout a wide range of environmental conditions (pH 4–9 for As^{III} and Sb^{III}, pH 5–7.5 for Se^{IV}, ionic strength 0.01–200 mmol L^{-1} NO_3^-) and has been validated to be robust for *in-situ* measuring As^{III}, Sb^{III}, and Se^{IV} in natural water systems. In addition to application in environmental monitoring at the hectometer scale, AMBS binding gel coupled with LA-ICPMS was effective in revealing 2D spatial patterns of As^{III}, Sb^{III}, and Se^{IV} in the environment with low disturbance and high resolution of μm–mm. When the AMBS-DGT was combined other DGT binding layers and some

non-invasive techniques for biogeochemical parameters, it could be promising to completely depict the distribution of different speciation and interpret the speciation transformation processes.

■ ASSOCIATED CONTENT

Supporting Information

The Supporting Information is available free of charge on the ACS Publications website at DOI:

Description of the DGT principal (Text S1); determination of diffusion coefficients (Text S2); HPLC-ICPMS methods to measure As, Se, and Sb speciation (Text S3); preparation of soil samples and rhizotrons (Text S4); LA-ICPMS measurement of element accumulation in binding gels (Text S5); DGT Blanks, Detection limits, and Elution efficiency of AMBS-DGT (Text S6); Aging Effect (Text S7); Diffusion Coefficients in Diffusive Gels (Text S8); standard calibrations for DGT-LA-ICPMS measurement (Figure S1); uptake kinetics for SBA-I and SBA-II binding gels (Figure S2); pH effects on As^{V}, Se^{VI}, Sb^{V} accumulation by SBA-II-DGT and AMBS-DGT (Figure S3); long-term mass accumulation of As, Se, and Sb by AMBS-DGT (Figure S4); accumulated masses of As^{III}, Sb^{III} and Se^{IV} by AMBS-DGT as a function of the solution concentrations (Figure S5); Diffusion curves of As^{III}, Se^{IV}, Sb^{III} through diffusive gels (Figure S6); performance of AMBS-DGT after different aging time (Figure S7); As^{III}, Sb^{III}, and Se^{IV} flux transect along the profile plot in the rice rhizosphere (Figure S8); characterization of AMBS, MFS, SBA materials by XPS

spectra (Table S1); DGT capacities (Table S2); DGT selectivity (Table S3); concentrations of different As, Sb, and Se species in grab water samples from field application (Table S4); instrumental parameters for LA-ICP-MS analysis (Table S5); DGT blanks and method detection limits (Table S6); elution efficiencies of As, Se, and As (Table S7).

■ AUTHOR INFORMATION

Corresponding Authors

*Phone: 0086−25−89680632; e-mail: esluojun@nju.edu.cn (J.L.).

Notes

The authors declare no competing financial interest.

■ ACKNOWLEDGMENTS

This work was funded by National Key Research and Development Plans of Special Project for Site soils (No. 2019YFC1805201, 2018YFC1800602, and 2018YFC1801002), the National Natural Science Foundation of China (No. 41807023, 41771271, 41977111, and 21637002), and Natural Science Foundation of Jiangsu Province (BK20180344).

■ REFERENCES

1. Rothwell, J. J.; Taylor, K. G.; Chenery, S. R. N.; Cundy, A. B.; Evans, M. G.; Allottt, T. E. H., Storage and Behavior of As, Sb, Pb, and Cu in Ombrotrophic Peat Bogs under Contrasting Water Table Conditions. *Environ. Sci. Technol.* **2010,** *44* (22), 8497-8502.
2. Yang, H.; He, M., Distribution and Speciation of Selenium, Antimony, and Arsenic in Soils and Sediments Around the Area of Xikuangshan (China). *Clean - Soil Air Water* **2016,** *44* (11), 1538-1546.
3. Sun, W.; Xiao, E.; Xiao, T.; Krumins, V.; Wang, Q.; Haggblom, M.; Dong, Y.; Tang, S.; Hu, M.; Li, B.; Xia, B.; Liu, W., Response of Soil Microbial Communities to

Elevated Antimony and Arsenic Contamination Indicates the Relationship between the Innate Microbiota and Contaminant Fractions. *Environ. Sci. Technol.* **2017,** *51* (16), 9165-9175.
4. Okkenhaug, G.; Zhu, Y. G.; He, J.; Li, X.; Luo, L.; Mulder, J., Antimony (Sb) and arsenic (As) in Sb mining impacted paddy soil from Xikuangshan, China: differences in mechanisms controlling soil sequestration and uptake in rice. *Environ. Sci. Technol.* **2012,** *46* (6), 3155-3162.
5. Chen, J.; He, W.; Zhu, X.; Yang, S.; Yu, T.; Ma, W., Epidemiological study of kidney health in an area with high levels of soil cadmium and selenium: Does selenium protect against cadmium-induced kidney injury? *Sci. Total Environ.* **2019,** *698*, 134106.
6. He, M.; Wang, N.; Long, X.; Zhang, C.; Ma, C.; Zhong, Q.; Wang, A.; Wang, Y.; Pervaiz, A.; Shan, J., Antimony speciation in the environment: Recent advances in understanding the biogeochemical processes and ecological effects. *Journal of environmental sciences* **2019,** *75*, 14-39.
7. Chen, J.; Liu, G.; Kang, Y.; Wu, B.; Sun, R.; Zhou, C.; Wu, D., Atmospheric emissions of F, As, Se, Hg, and Sb from coal-fired power and heat generation in China. *Chemosphere* **2013,** *90* (6), 1925-1932.
8. Peiffer, S.; Kappler, A.; Haderlein, S. B.; Schmidt, C.; Byrne, J. M.; Kleindienst, S.; Vogt, C.; Richnow, H. H.; Obst, M.; Angenent, L. T.; Bryce, C.; McCammon, C.; Planer-Friedrich, B., A biogeochemical–hydrological framework for the role of redox-active compounds in aquatic systems. *Nat. Geosci.* **2021,** *14* (5), 264-272.
9. Philippot, L.; Raaijmakers, J. M.; Lemanceau, P.; van der Putten, W. H., Going back to the roots: the microbial ecology of the rhizosphere. *Nat. Rev. Microbiol.* **2013,** *11* (11), 789-799.
10. Rakhunde, R.; Deshpande, L.; Juneja, H. D., Chemical Speciation of Chromium in Water: A Review. *Crit. Rev. Env. Sci. Tec.* **2012,** *42* (7), 776-810.
11. Sharma, V. K.; Sohn, M., Aquatic arsenic: toxicity, speciation, transformations, and remediation. *Environ. Int.* **2009,** *35* (4), 743-759.
12. Wei, X.; Zhu, Z.; Wei, L.; Wu, J.; Ge, T., Biogeochemical cycles of key elements in the paddy-rice rhizosphere: Microbial mechanisms and coupling processes. *Rhizosphere* **2019,** *10*, 100145.
13. Keiluweit, M.; Wanzek, T.; Kleber, M.; Nico, P.; Fendorf, S., Anaerobic microsites have an unaccounted role in soil carbon stabilization. *Nat. Commun.* **2017,** *8* (1).
14. Nel, A. E.; Madler, L.; Velegol, D.; Xia, T.; Hoek, E. M.; Somasundaran, P.; Klaessig, F.; Castranova, V.; Thompson, M., Understanding biophysicochemical interactions at the nano-bio interface. *Nat. Mater.* **2009,** *8* (7), 543-557.
15. Williams, P. N.; Santner, J.; Larsen, M.; Lehto, N. J.; Oburger, E.; Wenzel, W.; Glud, R. N.; Davison, W.; Zhang, H., Localized flux maxima of arsenic, lead, and iron around root apices in flooded lowland rice. *Environ. Sci. Technol.* **2014,** *48* (15), 8498-8506.
16. Yin, D. X.; Fang, W.; Guan, D. X.; Williams, P. N.; Moreno-Jimenez, E.; Gao, Y.; Zhao, F. J.; Ma, L. Q.; Zhang, H.; Luo, J., Localized Intensification of Arsenic Release within the Emergent Rice Rhizosphere. *Environ. Sci. Technol.* **2020,** *54* (6), 3138-3147.

17. Fang, W.; Shi, X.; Yang, D.; Hu, X.; Williams, P. N.; Shi, B.; Liu, Z.; Luo, J., In situ selective measurement based on Diffusive Gradients in Thin-Films technique with mercapto-functionalized mesoporous silica for high-resolution imaging of SbIII in soil. *Anal. Chem.* **2020**.
18. Somenahally, A. C.; Hollister, E. B.; Yan, W.; Gentry, T. J.; Loeppert, R. H., Water management impacts on arsenic speciation and iron-reducing bacteria in contrasting rice-rhizosphere compartments. *Environ. Sci. Technol.* **2011,** *45* (19), 8328-8335.
19. Jain, C. K.; Ali, I., Arsenic: Occurrence, toxicity and speciation techniques. *Water Res.* **2000,** *34* (17), 4304-4312.
20. Fang, W.; Williams, P. N.; Fang, X.; Amoah-Antwi, C.; Yin, D.; Li, G.; Ma, L. Q.; Luo, J., Field-Scale Heterogeneity and Geochemical Regulation of Arsenic, Iron, Lead, and Sulfur Bioavailability in Paddy Soil. *Environ. Sci. Technol.* **2018,** *52* (21), 12098-12107.
21. Bennett, W. W.; Teasdale, P. R.; Panther, J. G.; Welsh, D. T.; Jolley, D. F., Speciation of dissolved inorganic arsenic by diffusive gradients in thin films: selective binding of AsIII by 3-mercaptopropyl-functionalized silica gel. *Anal. Chem.* **2011,** *83* (21), 8293-8299.
22. Pan, Y.; Guan, D. X.; Zhao, D.; Luo, J.; Zhang, H.; Davison, W.; Ma, L. Q., Novel Speciation Method Based on Diffusive Gradients in Thin-Films for in Situ Measurement of Cr(VI) in Aquatic Systems. *Environ. Sci. Technol.* **2015,** *49* (24), 14267-14273.
23. Guan, D. X.; Williams, P. N.; Luo, J.; Zheng, J. L.; Xu, H. C.; Cai, C.; Ma, L. Q., Novel precipitated zirconia-based DGT technique for high-resolution imaging of oxyanions in waters and sediments. *Environ. Sci. Technol.* **2015,** *49* (6), 3653-61.
24. Shi, X.; Fang, W.; Tang, N.; Williams, P. N.; Hu, X.; Liu, Z.; Yin, D.; Ma, L. Q.; Luo, J., In Situ Selective Measurement of Se(IV) in Waters and Soils: Diffusive Gradients in Thin-Films with Bi-Functionalized Silica Nanoparticles. *Environ. Sci. Technol.* **2018,** *52* (24), 14140-14148.
25. Bennett, W. W.; Arsic, M.; Welsh, D. T.; Teasdale, P. R., In situ speciation of dissolved inorganic antimony in surface waters and sediment porewaters: development of a thiol-based diffusive gradients in thin films technique for Sb(III). *Environ. Sci. Proc. Imp.* **2016,** *18* (8), 992-998.
26. Krachler, M.; Emons, H.; Zheng, J., Speciation of antimony for the 21st century: promises and pitfalls. *Trac-Trend. Anal. Chem.* **2001,** *20* (2), 79-90.
27. Chand, V.; Prasad, S., Trace determination and chemical speciation of selenium in environmental water samples using catalytic kinetic spectrophotometric method. *J. Hazard. Mater.* **2009,** *165* (1-3), 780-8.
28. Aguado, J.; Arsuaga, J. M.; Arencibia, A., Influence of synthesis conditions on mercury adsorption capacity of propylthiol functionalized SBA-15 obtained by co-condensation. *Micropor. Mesopor. Mat.* **2008,** *109* (1-3), 513-524.
29. Burke, A. M.; Hanrahan, J. P.; Healy, D. A.; Sodeau, J. R.; Holmes, J. D.; Morris, M. A., Large pore bi-functionalised mesoporous silica for metal ion pollution treatment.

J. Hazard. Mater. **2009,** *164* (1), 229-234.
30. Davison, W.; Zhang, H., In-Situ Speciation Measurements of Trace Components in Natural-Waters Using Thin-Film Gels. *Nature* **1994,** *367* (6463), 546-548.
31. Zhang, H.; Davison, W., Performance Characteristics of Diffusion Gradients in Thin Films for the in Situ Measurement of Trace Metals in Aqueous Solution. *Anal. Chem.* **1995,** *67* (19), 3391-3400.
32. Peng, Y.; Fang, W.; Krauss, M.; Brack, W.; Wang, Z.; Li, F.; Zhang, X., Screening hundreds of emerging organic pollutants (EOPs) in surface water from the Yangtze River Delta (YRD): Occurrence, distribution, ecological risk. *Environ. Pollut.* **2018,** *241*, 484-493.
33. Yang, J.; Chai, L.; Li, Q.; Shu, Y., Redox behavior and chemical species of arsenic in acidic aqueous system. *Trans. Nonferrous Met. Soc. China* **2017,** *27* (9), 2063-2072.
34. Sharma, V. K.; McDonald, T. J.; Sohn, M.; Anquandah, G. A. K.; Pettine, M.; Zboril, R., Biogeochemistry of selenium. A review. *Environ. Chem. Lett.* **2014,** *13* (1), 49-58.
35. Walcarius, A.; Mercier, L., Mesoporous organosilica adsorbents: nanoengineered materials for removal of organic and inorganic pollutants. *J. Mater. Chem.* **2010,** *20* (22), 4478.
36. Fan, H.-T.; Liu, A.-J.; Jiang, B.; Wang, Q.-J.; Li, T.; Huang, C.-C., Sampling of dissolved inorganic SbIII by mercapto-functionalized silica-based diffusive gradients in thin-film technique. *RSC Adv.* **2016,** *6* (4), 2624-2631.
37. Kice, J. L.; Lee, T. W. S.; Pan, S., Mechanism of the Reaction of Thiols with Selenite. *J. Am. Chem. Soc.* **1980,** *102* (13), 4448-4455.
38. Luo, J.; Zhang, H.; Santner, J.; Davison, W., Performance characteristics of diffusive gradients in thin films equipped with a binding gel layer containing precipitated ferrihydrite for measuring arsenic(V), selenium(VI), vanadium(V), and antimony(V). *Anal. Chem.* **2010,** *82* (21), 8903-8909.
39. Zhang, H.; Davison, W., Diffusional characteristics of hydrogels used in DGT and DET techniques. *Anal. Chim. Acta* **1999,** *398* (2-3), 329-340.
40. Yezek, L. P.; van Leeuwen, H. P., An electrokinetic characterization of low charge density cross-linked polyacrylamide gels. *J. Colloid Interf. Sci* **2004,** *278* (1), 243-250.
41. Schmidt, H.; Eickhorst, T.; Tippkötter, R., Monitoring of root growth and redox conditions in paddy soil rhizotrons by redox electrodes and image analysis. *Plant Soil* **2010,** *341* (1-2), 221-232.
42. Xu, W. F.; Chen, Q. X.; Shi, W. M., Effects of nitrate supply site on selenite uptake by rice roots. *J. Agr. Food Chem.* **2010,** *58* (20), 11075-11080.
43. Hoefer, C.; Santner, J.; Puschenreiter, M.; Wenzel, W. W., Localized metal solubilization in the rhizosphere of Salix smithiana upon sulfur application. *Environ. Sci. Technol.* **2015,** *49* (7), 4522-9.
44. Yamaguchi, N.; Ohkura, T.; Takahashi, Y.; Maejima, Y.; Arao, T., Arsenic Distribution and Speciation near Rice Roots Influenced by Iron Plaques and Redox Conditions of the Soil Matrix. *Environ. Sci. Technol.* **2014,** *48* (3), 1549-1556.

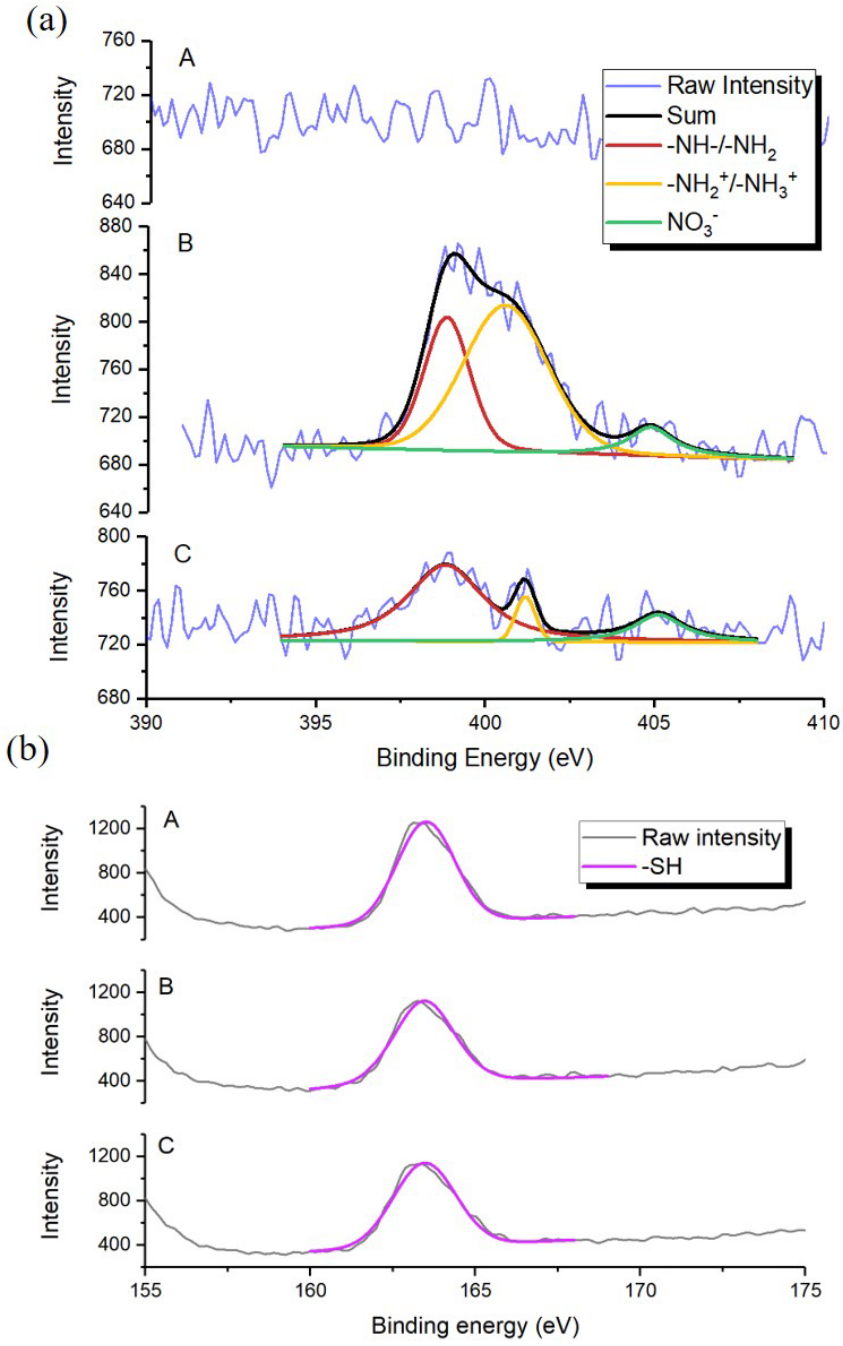

Figure 1. XPS spectra of the (a) N1s core level, (b) S2p core level, and corresponding fitted curves for A) SBA-I, B) SBA-II, and C) AMBS firstly synthesized in this study.

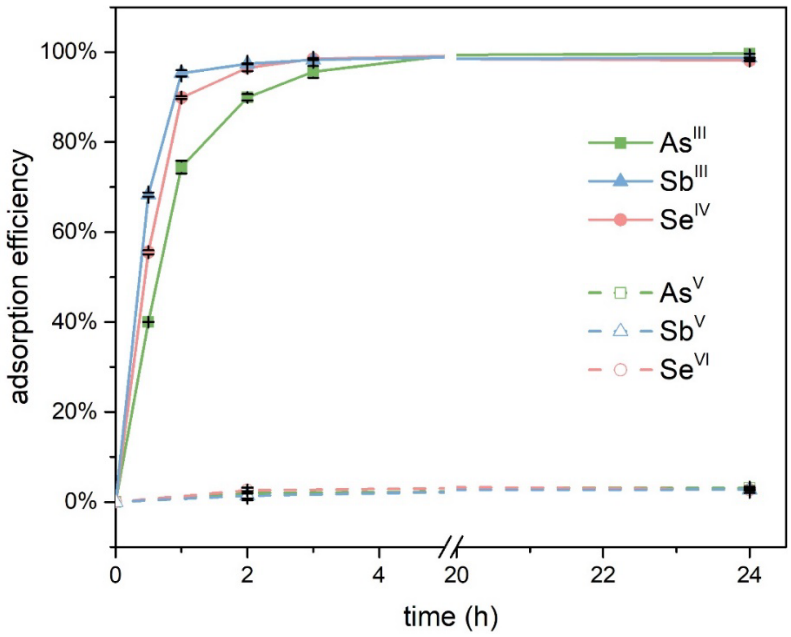

598

599 **Figure 2.** Uptake kinetics of As, Sb, and Se by AMBS binding gels immersed in 10 mL

600 of 0.01 mol L^{-1} $NaNO_3$ solutions containing ~50 µg L^{-1} As^{III}, Sb^{III}, and Se^{IV} or As^{V}, Sb^{V},

601 and Se^{VI}.

602

603

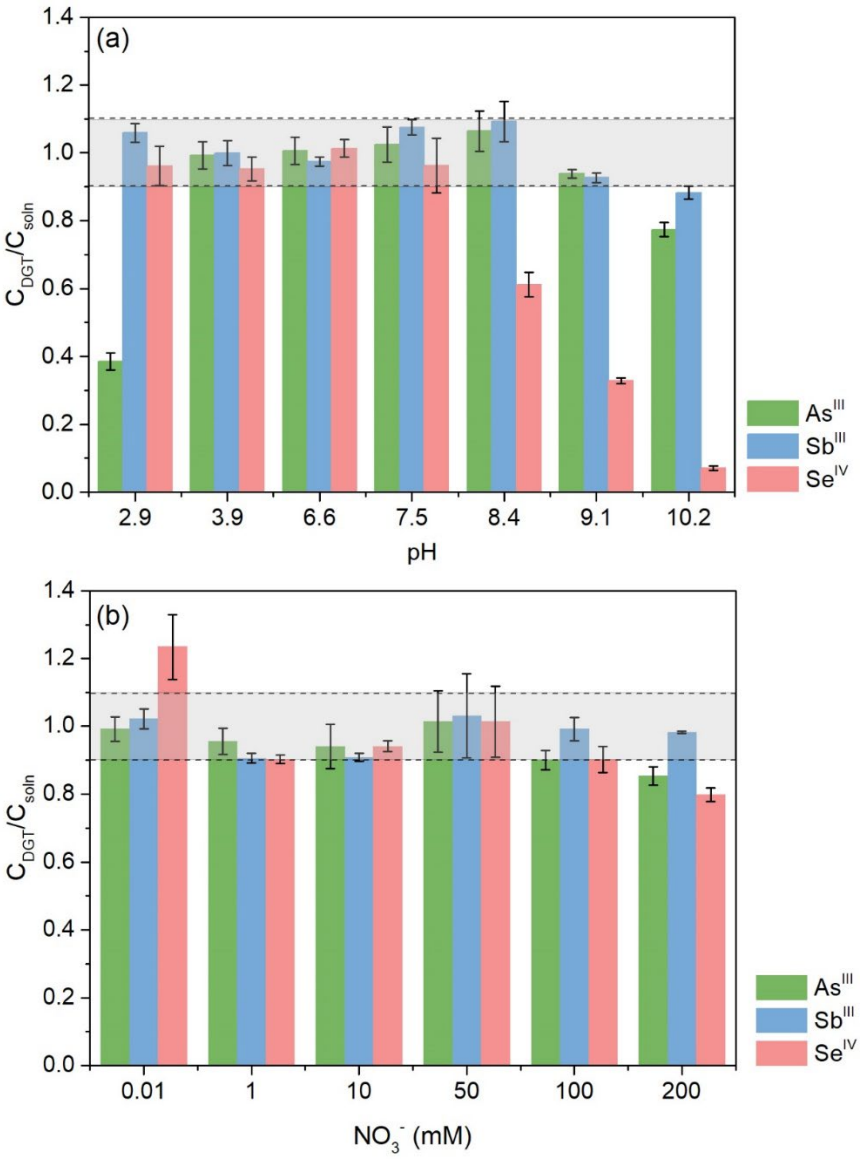

604

605 **Figure 3.** Effects of pH and ionic strength on the ratios of As^{III}, Sb^{III}, and Se^{IV}
606 concentrations measured by AMBS-DGT, C_{DGT}, to the concentrations, C_{soln}, of
607 deployment solution containing ~50 μg L^{-1} As^{III}, Sb^{III}, and Se^{IV} with the deployment
608 time of 4 h.

609

610

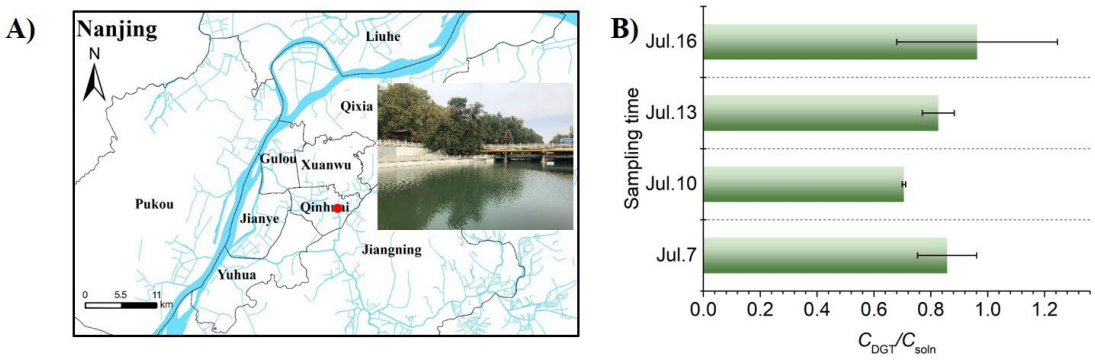

611

612 **Figure 4** (a) Map of sampling sites located in Nanjing, Jiangsu, China and (b) The ratio

613 of As^{III} concentrations measured by AMBS-DGT (C_{DGT}) in the field deployment to As^{III}

614 concentrations measured by grab sampling (C_{soln})

615

616

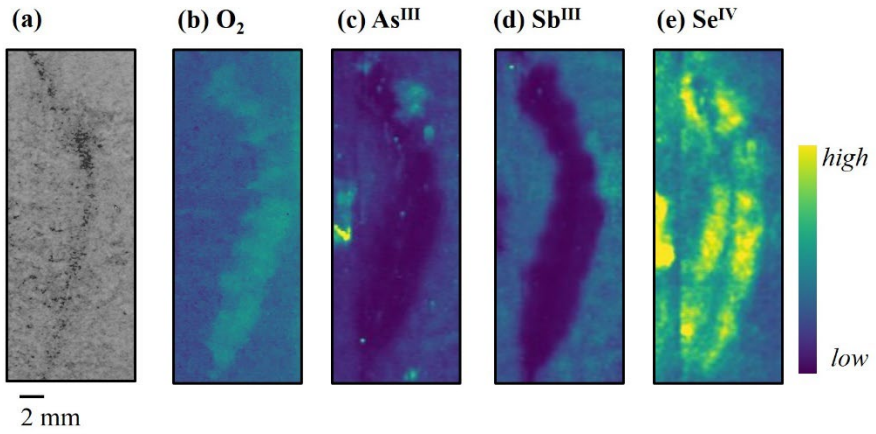

Figure 5. **As^{III}, Sb^{III}, and Se^{IV} lability in a set of living roots by AMBS-DGT/O_2 multilayer system.** (a) Photographic image of the root zone subjected to chemical imaging. (b) O_2 concentration distribution in the above root zone. (c) As^{III}, (d) Sb^{III}, and (e) Se^{IV} fluxes in the above root zone. The scales in the figures represent the following ranges from 0 to 1.23 pg cm^{-2} s^{-1} for As^{III}, from 0 to 2.59 pg cm^{-2} s^{-1} for Sb^{III}, and from 0 to 0.61 pg cm^{-2} s^{-1} for Se^{IV}.

627 **For TOC art only**

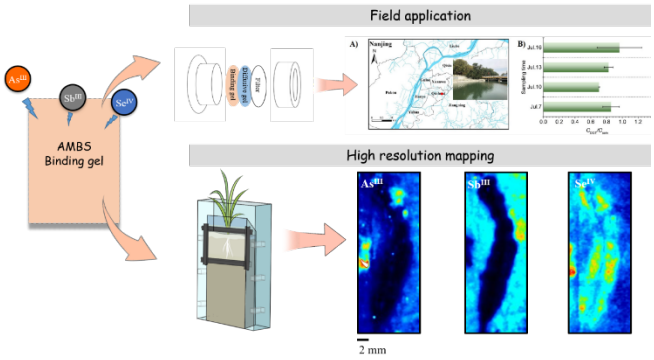

628

629